Interfacial design for reducing charge recombination in photovoltaics

Shinnosuke Hattori,[1,a)] Weiwei Mou,[1] Pankaj Rajak,[1] Fuyuki Shimojo,[1,2] and Aiichiro Nakano[1]
[1]*Collaboratory for Advanced Computing and Simulations, Department of Physics & Astronomy, Department of Chemical Engineering & Materials Science, and Department of Computer Science, University of Southern California, Los Angeles, California 90089-0242, USA*
[2]*Department of Physics, Kumamoto University, Kumamoto 860-8555, Japan*

(Received 18 December 2012; accepted 26 February 2013; published online 8 March 2013)

Key to high power conversion efficiency of organic solar cells is to minimize charge recombination (CR) at electron donor/acceptor interfaces. Here, nonadiabatic quantum molecular dynamics simulation shows how the interfacial structure can be controlled by molecular design at acene/C_{60} interfaces to suppress CR. Orders-of-magnitude reduction of the CR rate is achieved through drastic modification of interfacial structure by attaching phenyl groups to tetracene. This finding confirms a molecular design principle for efficient organic photovoltaics underlying a recent experimental study. © *2013 American Institute of Physics*. [http://dx.doi.org/10.1063/1.4794983]

Key to high power conversion efficiency of solar cells is to enhance charge transfer (CT) of photoexcited electrons from an electron donor material to an electron acceptor material at a donor/acceptor interface, but at the same time to minimize charge recombination (CR) back to the donor.[1] Finding an optimal combination of donor and acceptor molecules to simultaneously achieve these requirements is a major goal for the molecular design of organic solar cells. An archetypal example is tetracene (Tc)/C_{60} and rubrene (Rub)/C_{60} interfaces,[2] where the only difference between the Rub and Tc molecules is the four phenyl groups attached to the aromatic backbone in the former (Figs. 1(a) and 1(b)). Though the electronic energy levels and molecular orbitals responsible for the open-circuit voltage V_{oc} (which is proportional to power conversion efficiency[1]) are similar between Tc and Rub, the measured V_{oc}(Rub/C_{60}) is nearly twice as large as V_{oc}(Tc/C_{60}).[2] Our previous nonadiabatic quantum molecular dynamics (NAQMD) simulation of a single Tc or Rub molecule on a C_{60} (111) surface showed slight enhancement of phonon-assisted CT in Rub/C_{60} due to the amplification of breathing modes of aromatic rings by the phenyl groups over those in Tc/C_{60}.[3]

However, the enhanced CT rate alone is not sufficient to explain the experimentally observed large change in V_{oc}. Since the energy of photoexcited electrons in the donor is within the continuous conduction band of the acceptor solid, CT processes are less sensitive to the fluctuation of energy levels than CR processes.[4] Thus, CR processes are expected to play a major role. Another essential factor is the relative orientation of donor and acceptor molecules, which was shown to play an important role in these processes in a similar interface, i.e., pentacene/C_{60}.[5] The change of donor molecules (e.g., from tetracene to rubrene) often leads to a change in the donor/acceptor interfacial structure, which in turn could modify the CR rate. In fact, the CR rate was shown to be highly sensitive to the change in molecular conformations at donor/acceptor interfaces.[4]

Here, we study the effect of interfacial structures on the CR rate at Tc/C_{60} and Rub/C_{60} interfaces by combining molecular dynamics (MD) and NAQMD simulations, so as to provide a large sampling of interfacial molecular conformations. The simulation results reveal a drastic change of interfacial structure by the attachment of phenyl groups to tetracene, which reduces the CR rate by orders-of-magnitude. The atomistic mechanism of the reduced CR is found to be the steric size of the phenyl groups, which separates donor and acceptor molecules. This finding confirms a molecular design principle for efficient organic photovoltaics underlying a recent experimental work.[2]

We first perform MD simulations to prepare Tc/C_{60} and Rub/C_{60} interfaces by depositing tetracene or rubrene molecules on the (111) surface of C_{60} face-centered-cubic crystal, followed by a melt-quench procedure to anneal the interfacial structure.[3] The simulation box of dimensions $68 \times 78 \times 140$ Å^3 contains 320 C_{60} molecules and 216 tetracene molecules (or 160 rubrene molecules). The total number of atoms is 25 680 or 30 400, respectively, for the Tc/C_{60} or Rub/C_{60}

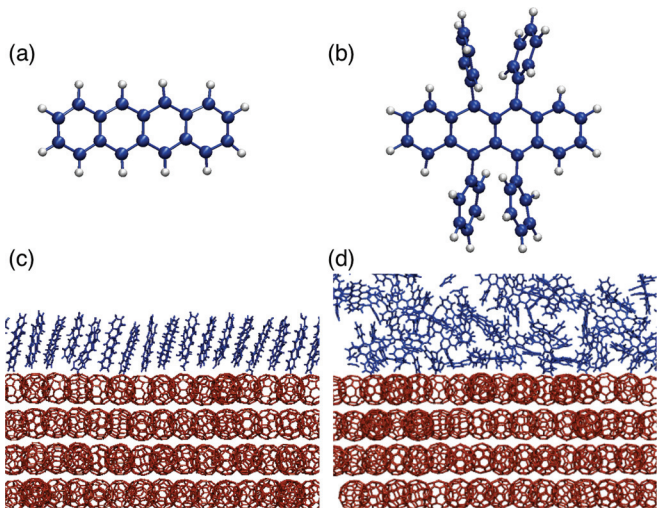

FIG. 1. (a) Tetracene and (b) rubrene molecules, where C and H atoms are colored in blue and gray, respectively. (c) Tetracene (blue) and (d) rubrene (blue) deposited on C_{60} (111) surface (red).

[a)]Present address: Sony Corporation, Atsugi-shi, Kanagawa 243-0021, Japan.

system. Periodic boundary conditions are applied to all Cartesian directions, and a vacuum layer of thickness 100 Å is inserted in the z direction (which is parallel to the [111] axis of C_{60} crystal) to prevent periodic images from interacting. We use the general Amber force field,[6] and the Nosé-Hoover thermostat is employed for temparature control during the melt-quench procedure. We first melt tetracene (or rubrene) at a temperature of 700 K on the C_{60} (111) surface. The temperature is then lowered from 700 to 300 K within 10 ns, and the system is thermalized at 300 K for 200 ps. Subsequently, statistical analysis is made for 200 ps, during which MD simulation is performed in the microcanonical ensamble. After the quench and thermalization procedudes, the root mean square and energy of the system is well stabilized. Previous MD simulation showed that a similar system size as used here is sufficient for sampling key short- and intermediate-range structural features.[7] In the subsequent analysis, the final MD configuration is used to sample the geometry of donor-acceptor dimers (182 Tc-C_{60} and 58 Rub-C_{60} dimers, respectively, at the Tc/C_{60} and Rub/C_{60} interfaces), which provides a sufficient sample size to characterize key structural features as discussed below.

Figures 1(c) and 1(d) show side views of the resulting Tc/C_{60} and Rub/C_{60} interfacial structures, respectively. The Tc/C_{60} interface in Fig. 1(c) is crystalline, with Tc molecules standing up in a head-on orientation. On the other hand, the Rub/C_{60} interface in Fig. 1(d) is highly disordered. These interfacial structures are different from those in our previous study,[3] in which a submonolayer of deposited film consisted of molecules with their backbone aromatic rings facing parallel to the surface (i.e., face-on orientation). The face-on to head-on structural transformation of the Tc/C_{60} interface at increased layers of deposition is similar to that observed in previous MD study of pentacene/C_{60}.[8] This structural transformation is likely to arise from the competition between donor (Tc or Rub)-acceptor (C_{60}) and donor-donor molecular interactions: At a low deposition of donor molecules, the interfacial geometry minimizes the donor-acceptor interaction energy through the face-on donor orientation to maximize the donor-acceptor interaction; whereas at a higher deposition, the donor-donor interaction energy becomes dominant, and thus the head-on orientation is realized to maximize the number of donor-donor π-orbital interactions. In contrast to the crystalline Tc/C_{60} interface, the disordered Rub/C_{60} interface is likely due to frustrated crystal growth caused by the side phenyl groups.

To quantify the interfacial structures, we first calculate the distribution of the distance between the donor and acceptor molecules. Here, the distance is between the center-of-mass (COM) of the C atoms in the aromatic backbone (i.e., a fused four benzene rings) of a donor (tetracene or rubrene) molecule and the xy-plane containing the topmost C atom in the C_{60} crystal; see Fig. 2(a). Figure 2(b) shows the calculated histogram of donor-acceptor COM distance along the z-axis for Tc/C_{60} and Rub/C_{60} interfaces. The tetracene histogram exhibits a sharp single peak, signifying a crystalline monolayer of deposited tetracene molecules on C_{60} (111) surface. In contrast, the rubrene histogram has multiple broad peaks that are merged together, reflecting disordered deposition of multiple layers of rubrene molecules.

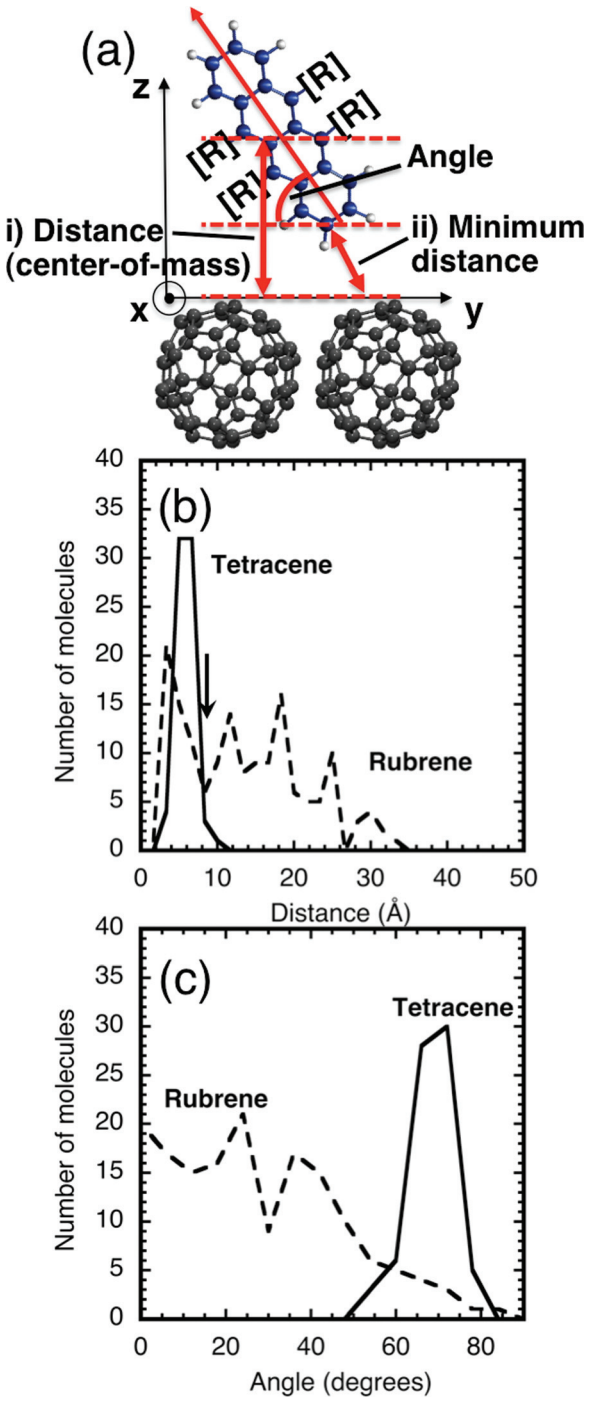

FIG. 2. (a) Schematic of the angle and distance between donor and acceptor molecules, where R stands for H atom for tetracene and phenyl group for rubrene. We define two distances: (i) the COM z coordinate of a donor molecule, for which the origin is the C_{60} surface; and (ii) the minimum C-C distance between donor and C_{60} molecules. (b) Histogram of COM distance from the surface of C_{60}(111) for both Tc/C_{60} and Rub/C_{60}, where the arrow indicates the maximum distance for the first deposited monolayer. (c) Angle histogram for both Tc/C_{60} and Rub/C_{60}.

We next characterize the angle of deposited donor molecules. Here, the angle is defined between the long axis of the backbone plane of a donor molecule and the C_{60} (111) surface; see Fig. 2(a). Figure 2(c) shows the calculated angle distribution for Tc/C_{60} and Rub/C_{60} interfaces. The tetracene angle distribution has a sharp peak around 70°, reflecting the highly aligned head-on conformation of tetracene molecules as shown in Fig. 1(c). In contrast, the rubrene angle is distributed broadly

between 0° and 90°. This is a consequence of highly disordered interfacial structure of Rub/C_{60} as shown in Fig. 1(d).

In order to study how the different structures between Tc/C_{60} and Rub/C_{60} interfaces in Fig. 2 influence the CR process, we first obtain the electronic ground states in the framework of density functional theory (DFT) using the plane-wave representation of Kohn-Sham (KS) orbitals and a hybrid exchange-correlation functional[9] involving the long-range nonlocal exact exchange correction.

For each tetracene or rubrene molecule in the first layer of the wetting film in the MD configuration, we perform DFT calculation for a dimer of tetracene (or rubrene) and C_{60} molecules by selecting the closest C_{60} from the configuration. In case of the Rub/C_{60} system, the first wetting layer is defined to be below the first minimum of the donor-acceptor COM distance histogram pointed to by the arrow in Fig. 2(b). Figures 3(a) and 3(b) show partial electronic density-of-states (DOS) for Tc/C_{60} and Rub/C_{60} systems, respectively, where an ensemble average is taken over all donor-acceptor dimers. The partial DOS is obtained by projecting each KS wave function to subsystems (i.e., tetracene, rubrene, and C_{60}). Figure 3 correctly describes the staggered type-II alignment among the highest occupied molecular orbitals (HOMO) and lowest unoccupied molecular orbitals (LUMO) of the donors (Tc or Rub) and the acceptor (C_{60}): (1) HOMO(Tc or Rub) lies between LUMO(C_{60}) and HOMO(C_{60}) (i.e., within the C_{60} band gap), while LUMO(Tc or Rub) falls within the C_{60} conduction band; and (2) the C_{60} conduction band is divided into the lowest (T_{1u}) and the next higher (T_{1g}) sub-bands, in agreement with previous theory and experiments.[10]

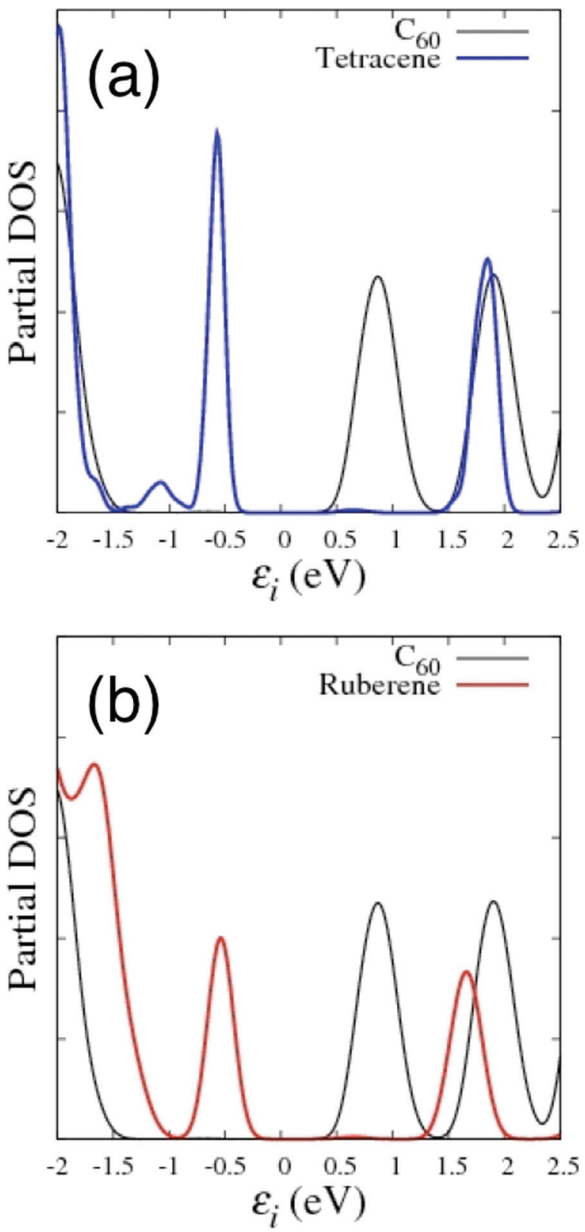

FIG. 3. Partial electronic density of states for (a) Tc/C_{60} and (b) Rub/C_{60} systems, where blue, red, and black curves are for Tc, Rub, and C_{60} subsystems, respectively.

Next, we perform NAQMD simulations[4,11–18] to calculate CR rates for all donor/acceptor dimers in the first deposition monolayer. We describe excited electronic states within Casida's linear-response time-dependent density functional theory,[19] using the ground-state KS orbitals as a basis set. Transitions between these excited states are described by Tully's fewest-switches surface-hopping method.[20] Interatomic forces are computed quantum mechanically for the excited electronic state for the current nuclear positions. A series of techniques are employed for efficiently calculating long-range exact exchange correction[9] and excited-state forces. The simulation program is parallelized using hybrid spatial and band decomposition. Detailed description of our NAQMD simulation code is given in Ref. 21.

Starting from each MD configuration, NAQMD simulations are performed to calculate the transition probability $\gamma_{ij}(t)$ from the current excited state i to another j as a function of time. The phonon-assisted CR rate is then estimated as $k_{CR} = \gamma_{\mathrm{LUMO(C60),HOMO(Tc\,or\,Rub)}}(t)/t$, respectively. Figure 4 shows the calculated CR rates as a function of the minimum donor-acceptor distance for all Tc/C_{60} (blue circles) and Rub/C_{60} (red crosses) dimers. For each donor molecule, the minimum distance is defined as the lowermost z coordinate of the backbone C atoms, where $z = 0$ is defined as the position of the topmost C atom in the C_{60} crystal; see Fig. 2(a). Overall, the CR rate is an exponentially decreasing function of the minimum donor-acceptor distance due to the decreasing overlap

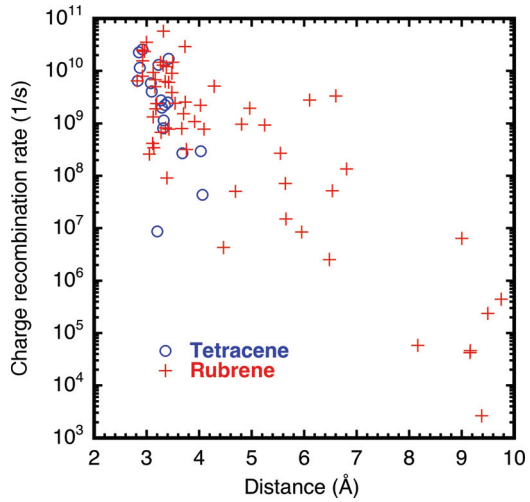

FIG. 4. Calculated CR rates from tetracene (open circle) and rubrene (cross) to C_{60} as a function of the minimum C-C distance between the aromatic backbone plane of the donor and acceptor molecules.

between donor and acceptor wave functions. Due to the broader distribution of the distance, the CR rates in Rub/C_{60} take smaller values on average. The harmonic mean of the CR rate is $1.2 \times 10^8\,s^{-1}$ and $1.3 \times 10^5\,s^{-1}$, respectively, for Tc/C_{60} and Rub/C_{60}. It is worth noting that the distance between the center-of-mass of a donor molecule in the first wetting layer and C_{60} surface is similar in both Tc/C_{60} and Rub/C_{60} systems. Namely, it is centered around 5 Å; see the first peaks of the tetracene and rubrene histograms in Fig. 2(b). However, the electronic coupling responsible for CR depends on a different donor/acceptor distance, i.e., the minimum distance between the aromatic backbone of a donor molecule (on which electronic π orbitals are distributed) and an acceptor surface. This minimum donor/acceptor distance clearly exhibits a negative correlation with the CR rate in Fig. 4, and the larger minimum distance on average for Rub/C_{60} results in the lower CR rate compared to that in Tc/C_{60}. This is likely due to the steric size of side phenyl groups, which separates the backbone aromatic plane of a donor from an acceptor molecule. It is worth noting that, in contrast to the CR rate, the CT rate has been shown to be less sensitive to such interfacial molecular geometry.[4] This is because the donor LUMO level involved in CT is located within the densely populated conduction band of the acceptor, and thus donor's LUMO is highly hybridized with excited orbitals in the acceptor.

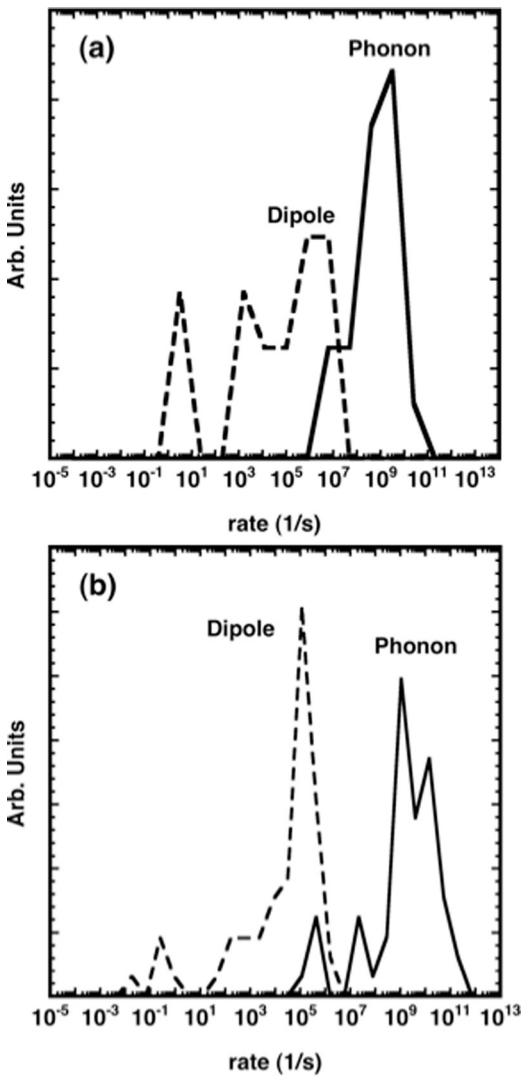

FIG. 5. CR rate distribution due to phonon (solid lines) and dipole (dashed lines) contributions in Tc/C_{60} (a) and Rub/C_{60} (b) interfaces.

In addition to the phonon-assisted CR rate in Fig. 4, we calculate the CR rate due to spontaneous emission based on the transition dipole moment approximation.[17] Figures 5(a) and 5(b) show histograms of phonon-assisted (solid lines) and dipole (dashed lines) CR rates for Tc/C_{60} and Rub/C_{60}, respectively. In both systems, the dipole contribution is orders-of-magnitude smaller than the phonon contribution. Thus, CR in Tc/C_{60} and Rub/C_{60} is dominated by phonon-assisted processes.

In summary, we have performed combined MD and NAQMD simulations to determine the effect of interfacial structures on charge recombination at tetracene/C_{60} and rubrene/C_{60} interfaces. The simulation results reveal a drastic change of interfacial structure by attaching phenyl groups to tetracene, which reduces the CR rate by orders-of-magnitude. This is mainly due to the enlargement of the donor/acceptor distance due to the steric size of side phenyl groups. This along with the dynamically enhanced CT rate in our previous study[3] may partly explain the higher open-circuit voltage V_{oc}(Rub/C_{60}) compared to V_{oc}(Tc/C_{60}) observed experimentally.[2] The atomistic mechanisms found here shed some light on better molecular structure design for efficient solar cells. Such molecular-level considerations complement calculations of various rates relevant for the power efficiency of solar cells.[22,23] The resulting atomistic understanding is expected to augment a comprehensive kinetic modeling of organic solar cells,[24] thereby paving a way to first-principles nanostructural design of highly efficient solar cells.

This work was supported by the U.S. Department of Energy (DOE), Office of Science, under Award DE-FG02-04ER46130. Performance optimization of the simulation code was supported by the DOE SciDAC-e Award DE-FC02-06ER25765. W.M. was supported by the Center for Energy Nanoscience, a DOE Energy Frontier Research Center under Award DE-SC0001013. Simulations were performed at the University of Southern California using the 20925-processor Linux cluster at the High Performance Computing Facility.

[1]C. W. Schlenker and M. E. Thompson, in *Topics in Current Chemistry* (Springer, Berlin, 2011), pp. 1–38.
[2]M. D. Perez, C. Borek, S. R. Forrest, and M. E. Thompson, J. Am. Chem. Soc. **131**(26), 9281–9286 (2009).
[3]W. Mou, S. Ohmura, S. Hattori, K. Nomura, F. Shimojo, and A. Nakano, J. Chem. Phys. **136**(18), 184705 (2012).
[4]W. Mou, S. Ohmura, F. Shimojo, and A. Nakano, Appl. Phys. Lett. **100**(20), 203306 (2012).
[5]Y. P. Yi, V. Coropceanu, and J. L. Bredas, J. Am. Chem. Soc. **131**(43), 15777–15783 (2009).
[6]J. M. Wang, R. M. Wolf, J. W. Caldwell, P. A. Kollman, and D. A. Case, J. Comput. Chem. **25**(9), 1157–1174 (2004).
[7]A. Nakano, R. K. Kalia, and P. Vashishta, J. Non-Cryst. Solids **171**(2), 157–163 (1994).
[8]L. Muccioli, G. D'Avino, and C. Zannoni, Adv. Mater. **23**(39), 4532–4536 (2011).
[9]Y. Tawada, T. Tsuneda, S. Yanagisawa, T. Yanai, and K. Hirao, J. Chem. Phys. **120**(18), 8425–8433 (2004).
[10]E. L. Shirley and S. G. Louie, Phys. Rev. Lett. **71**(1), 133–136 (1993).
[11]N. L. Doltsinis and D. Marx, Phys. Rev. Lett. **88**(16), 166402 (2002).
[12]C. F. Craig, W. R. Duncan, and O. V. Prezhdo, Phys. Rev. Lett. **95**(16), 163001 (2005).

[13]E. Tapavicza, I. Tavernelli, and U. Rothlisberger, Phys. Rev. Lett. **98**(2), 023001 (2007).
[14]C. P. Hu, H. Hirai, and O. Sugino, J. Chem. Phys. **127**(6), 064103 (2007).
[15]S. Ohmura, S. Koga, I. Akai, F. Shimojo, R. K. Kalia, A. Nakano, and P. Vashishta, Appl. Phys. Lett. **98**(11), 113302 (2011).
[16]S. Meng and E. Kaxiras, J. Chem. Phys. **129**(5), 054110 (2008).
[17]X. Zhang, Z. Li, and G. Lu, Phys. Rev. B **84**(23), 235208 (2011).
[18]C. Lv, X. J. Wang, G. Agalya, M. Koyama, M. Kubo, and A. Miyamoto, Appl. Surf. Sci. **244**(1–4), 541–545 (2005).
[19]M. E. Casida, in *Recent Advances in Density Functional Methods (Part I)*, edited by D. P. Chong (World Scientific, Singapore, 1995), pp. 155–192.
[20]J. C. Tully, J. Chem. Phys. **93**(2), 1061–1071 (1990).
[21]F. Shimojo, S. Ohmura, W. Mou, R. K. Kalia, A. Nakano, and P. Vashishta, Comput. Phys. Commun. **184**(1), 1–8 (2013).
[22]L. W. Wang, Energy Environ. Sci. **2**(9), 944–955 (2009).
[23]Y. Fu, Y. H. Zhou, H. B. Su, F. Y. C. Boey, and H. Agren, J. Phys. Chem. C **114**(9), 3743–3747 (2010).
[24]N. C. Giebink, G. P. Wiederrecht, M. R. Wasielewski, and S. R. Forrest, Phys. Rev. B **82**(15), 155305 (2010).